View Online / Journal Homepage
Dynamic Article Links

Soft Matter

Cite this: DOI: 10.1039/c1sm06563g

www.rsc.org/softmatter

PAPER

Force spectroscopy of Rev-peptide–RRE interaction from HIV-1

Jelena Živković,[a] Luuk Janssen,[b] Fresia Alvarado,[a] Sylvia Speller†[a] and Hans A. Heus†*[b]

Received 16th August 2011, Accepted 17th October 2011
DOI: 10.1039/c1sm06563g

The specific interaction of the RNA recognition motif of Rev and its viral mRNA target, RRE, has been demonstrated for the first time at the single-molecule level by atomic-force-microscope based single-molecule-force-spectroscopy (AFM-SMFS). The approach reveals details of the dissociation pathway and contribution of base mutations. Specific RNA–protein interaction is efficiently blocked by the RNA binding agent neomycin, showing the potential of AFM-SMFS as an efficient tool for single-molecule drug screening of RNA targets. Furthermore, we show the importance of surface chemistry in AFM-SMFS of RNA–protein interaction, in particular the influence of polymer linkers.

1. Introduction

Ever since AFM was recognized as a powerful tool for obtaining novel information of molecular properties by measuring unbinding forces, it has been employed to describe various biomolecular interactions such as DNA–protein, DNA–DNA, and ligand–receptor interactions.[1–3] By attaching complementary biomolecules on a solid support and to an AFM cantilever, unbinding forces between individual partners can be measured, from which relevant kinetic parameters of bond dissociation can be derived. Furthermore, combined with its ability to scan a surface and measure forces at the same time, AFM holds great promise for development of binding assays for drug screening at the single-molecule level. Despite the omnipresent functional importance of RNA–protein complexes and the unique potential of RNA as a novel drug target, only a few reports so far describe the use of AFM force spectroscopy for characterizing RNA–protein interaction.[4,5]

RNA–protein complexes play essential roles in nearly every aspect of cellular development, including, *e.g.*, RNA processing, mRNA translation, transcriptional control, and chromosome maintenance. In addition, RNA serves as the genome of many viruses, such as HIV-1, whose replication cycle depends strongly on two sequence specific RNA–protein interactions: TAR–Tat and RRE–Rev.[6,7] By targeting the RNA moiety, the specificity of these interactions provides new leads for drug discovery with the rationale to find small molecules that block formation of RNA–protein complexes crucial for viral replication.

Rev is an essential regulatory protein of HIV-1 that controls production of viral proteins, required for the assembly of infectious virions.[6–10] In the absence of Rev, shortly after infection of cells, HIV-mRNAs are fully spliced and exported from the nucleus to the cytoplasm for the synthesis of the regulatory proteins Rev, Tat and Nef. Rev shuttles back to the nucleus, where it protects viral mRNA from the host cell's splicing machinery and activates nuclear export of nonspliced and partially spliced mRNAs that encode for the structural proteins.[8–10] To achieve this Rev binds to an ~351 nucleotide RNA stem-loop structure, termed the Rev responsive element (RRE), which is encoded within the HIV-1 env gene. Rev first binds to a site, containing a purine rich internal loop located in the stem-loop IIB region of RRE, followed by multimerization of other Rev proteins along RRE.[10] Stem loop IIB is the most preserved sequence along all HIV isolates and mutational studies of RRE have shown that binding of Rev to RRE is highly sequence specific.[11,12] So far the only high-resolution information available is an NMR-based structure of the arginine-rich motif (ARM, residues 34–50 of Rev) bound to stem-loop IIB.[13] In this complex the ARM forms an α-helix, which donates several specific hydrogen bonds to essential residues in the stem-loop IIB bulge. To further characterize RNA–protein interaction by AFM-SMFS and develop AFM-based methodology for single-molecule drug screening, we investigated the RRE–Rev complex and probed the influence of the antibiotic neomycin B known to inhibit formation of the complex.[14,15]

2. Materials and methods

2.1 RNA synthesis

RNA oligonucleotides with 5′-hexanethiol label were synthesized using phosphoramidite chemistry (IBA, Germany). RNA sequences, constituting either wild type or mutated high affinity site, were extended on the 5′-end with a stretch of five adenines to

[a]*Scanning Probe Microscopy Group, Institute for Molecules and Materials, Radboud University, Nijmegen Heyendaalseweg 135, 6525 AJ Nijmegen, The Netherlands*
[b]*Department of Biophysical Chemistry, Institute for Molecules and Materials, Radboud University, Heyendaalseweg 135, 6525 AJ Nijmegen, The Netherlands. E-mail: H.Heus@science.ru.nl; Fax: +31 24-365-2112; Tel: +31 24-3653113*
† These authors contributed equally.

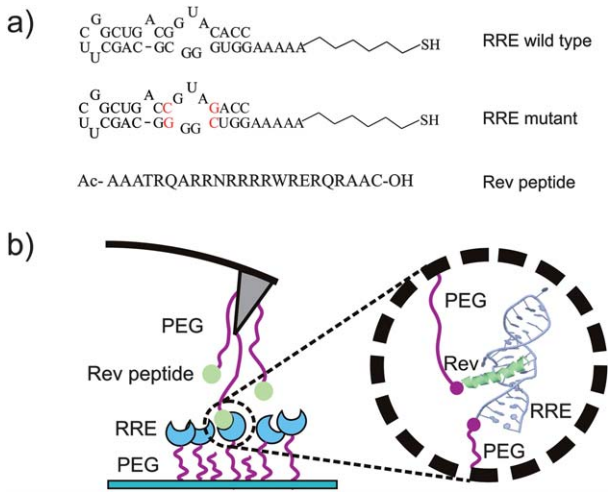

Fig. 1 (a) RNA and Rev peptide sequences used in this study. (b) Experimental setup. In the blow-up attachment of RNA and peptide to surface or cantilever *via* PEG spacers and complex formation is illustrated by the NMR-derived structure of the Rev–ARM stem-loop IIB complex.[13]

reduce nonspecific PEG–surface interaction. Full sequences are presented in Fig. 1(a).

2.2 Peptide synthesis

Rev peptide (Fig. 1(a)), modified on the *C*-terminus with cysteine, was synthesized by standard f-moc based solid phase peptide synthesis. Peptide samples were dissolved (20 mM) in coupling buffer (50 mM $NaPO_4/NaH_2PO_4$, 50 mM NaCl, pH 6.8) and stored at −20 °C. Before applying the peptide to amine-modified or PEG-coated AFM cantilevers, peptide was reduced by immobilized TCEP (tris-2-carboxyethyl-phosphine) disulfide gel (Pierce) according to the manufacturers protocol.

2.3 RNA and peptide immobilization

Procedures for RNA and peptide immobilization are based on protocols described in ref. 16–18. AFM tips (MLCT-AUHW, Veeco Instruments, Santa Barbara CA, USA) were activated by UV cleaning for 10 minutes and subsequently amino-functionalized with 3-aminopropyldimethyl-ethoxysilane (ABCR, Karlsruhe, Germany) as provided by the supplier without dilution. Afterwards they were washed with toluene (Sigma-Aldrich) and Milli-Q water and cured for 30 minutes at 80 °C. Ultrasonic and UV-cleaned glass slides (Menzel Gläser, Braunschweig, Germany) were silanized by incubating in a droplet of the same silane for 30 minutes, washed with isopropanol and cured for 1 hour at 80 °C. After silanization, cantilevers and glass slides were immersed in borate buffer for 1 hour to ensure free functional amino groups. Hetero-bifunctional NHS-PEG5000-Mal spacers (~50 nm, Rapp polymere, Karlsruhe, Germany) were dissolved at 50 mM in 50 mM sodium borate buffer pH 8.5. Cantilevers were incubated in a 50 µl droplet and glass slides were treated with a 50 µl droplet of dissolved PEG spacers for 1 hour at room temperature in a humid chamber. Hexanethiol modified RNAs were reduced by TCEP bond breaker (10 mM, Pierce), washed by ethanol precipitation and dissolved at ~30 µM in coupling buffer (50 mM $NaPO_4/NaH_2PO_4$, 50 mM NaCl, pH 6.8). Reduced RNAs were coupled with PEG-modified glass slides by adding a 25–30 µl droplet of dissolved RNA and leaving it to incubate overnight at 4 °C. Cantilevers were incubated overnight at 4 °C in a 25 µl droplet of ~0.4 mM reduced Rev peptide solution in coupling buffer. Cantilevers and glass slides were washed with measuring buffer (20 mM Tris, 100 mM KCl, pH 6.8) and stored in measuring buffer until use.

Gold surfaces were prepared according to the protocol described in ref. 19 and 20. For immobilization RNA oligos with 5′-hexanethiol label were deposited on a gold surface in a droplet (~ 20 µl) of RNA solution (100 µM) dissolved in sterile Milli-Q water.

2.4 Single molecule force measurements

Force measurements were done on a Veeco multimode AFM with a nanoscope IV controller (Veeco, Santa Barbara, CA, USA) using a contact mode liquid cell. Spring constants of the cantilevers (MLCT-AUHW, Veeco) were 0.017–0.06 N m^{-1} (C and D cantilevers) as determined by the thermal tune method.[21,22] Measurements were done with different retract velocities ranging from ~500 nm s^{-1} to 3.1 µm s^{-1}. The trigger set point for deflection of the cantilever was varied from 0.18 to 1.5 nN, and the surface delay time was set to either 0 or 120 ms. Measurements were done in standard buffer (20 mM Tris–HCl, 100 mM KCl, pH 6.8) in the absence or presence of neomycin B (100 mM, Sigma-Aldrich). For each velocity typically 1000 force–distance curves were measured. The yield of force curves showing relevant rupture events was usually between 25 and 30%. Each force and loading rate histogram was fitted with a probability density function which most reliably describes the dataset. Apart from surface chemistry (measurements using gold surfaces or PEG spacers for RNA immobilization) experimental conditions and the number of measurements were comparable.

2.5 Data analysis

Data analysis was done with MATLAB R2008 using a home-built program with a graphical user interface (GUI). The GUI allows individual inspection of each curve and marking the unbinding events. In cases when more than one single binding event was registered on the curve, only the last rupture was taken into statistical analysis. The loading rate (r) at the rupture event was determined by calculating the slope of the curve just before the rupture ($r = v\mathrm{d}F/\mathrm{d}z$). Values of rupture forces and corresponding loading rates were collected for each retract velocity separately and plotted in histograms.

2.6 Dynamic force spectroscopy

Rupture forces of the RRE–Rev interaction were measured with retraction velocities ranging from 581 nm s^{-1} to 3.1 µm s^{-1}. Typically, 1000 force curves were measured for each velocity. Most probable forces and most probable loading rates were then plotted in a semilogarithmic plot, the so-called dynamic force plot, which is used to estimate the bond parameters according to Bell's model.[23,24] The semilogarithmic plot of the most probable

rupture force against most probable loading rate was fitted linearly with the function:[23,24]

$$F^* = \frac{k_B T}{\Delta x} \ln \frac{\Delta x r}{k_B T k_{off}}$$

where F^* denotes the most probable rupture force, r the corresponding loading rate dF/dt, k_B Boltzmann's constant, T the absolute temperature, Δx the potential width scale, and k_{off} the dissociation rate constant at zero applied force.

The dataset where RRE was immobilized on a gold surface was additionally evaluated with the model proposed by Raible *et al.*[25] In contrast to Bell's model which relies on the force histograms and most probable values, the model introduced by Riable *et al.* is based on the analysis and fitting of $-v\log(pN_E)$ plots obtained from the experimental survival probability (pN_E) with the theoretical model described below. First the experimentally obtained survival probability pN_E was approximated by

$$pN_E = \frac{1}{n}\sum_{i=1}^{n} \Theta(F_i - F)$$

where n is the number of rupture events and $\Theta(F_i - F)$ represents the Heaviside step function. Subsequently, experimental curves $-v\ln(pN_E)$ for different retract velocities were created and fitted with the theoretical model:

$$-v\ln\left(p\overline{N}_T(F;\alpha)\right) = \int_{F_{min}}^{F} \frac{k_{off}\exp(\alpha F')}{k} dF'$$

where α represents the potential width in units of thermal energy ($\Delta x/k_B T$) and κ the effective spring constant of the cantilever-linker-molecule system, which was taken as the maximum of the distribution of all effective spring constants measured (κ = 0.0026 N m^{-1}). The term $p\bar{N}_T(F;\alpha)$ represents the theoretical survival probability averaged over parameter α given by a Gaussian distribution:

$$\rho(\alpha;\alpha_\mu;\sigma_\alpha) = Ce^{-(\alpha-\alpha_\mu)^2/2\sigma_\alpha^2}\Theta(\alpha)$$

The averaged survival probability was obtained according to ref. 25:

$$p\overline{N}_T(F;\alpha) = \frac{\int d\alpha \rho(\alpha;\alpha_\mu;\sigma_\alpha) pN_T(F;\alpha)}{\int d\alpha \rho(\alpha;\alpha_\mu;\sigma_\alpha) pN_T(F_{min};\alpha)}$$

The parameters k_{off}, α_μ and σ_α were varied to obtain the best fit evaluated by the error function:

$$E(\alpha_\mu,\sigma_\alpha) = \sum_{i=1}^{n}\left[pN_E(F_i) - p\overline{N}_T(F_i,\alpha_\mu,\sigma_\alpha)\right]^2$$

The error function was minimized for each retract velocity separately. After the parameters k_{off}, α_μ and σ_α were obtained for each velocity separately, their average values were calculated. This step represents a small deviation from the original error estimate used in the model of Raible *et al.*[25] and insures better fitting of the theoretical to experimental curves.

3. Results and discussion

3.1 AFM based SMFS of Rev–RRE

The interaction pair we used for this study is the small arginine-rich RNA binding motif of Rev (residues 34–51) and RNA hairpins containing the high-affinity site, which is a validated *in vitro* model system to characterize binding properties.[26,27] We engineered two RNA hairpins containing either wild type or mutated high-affinity site and probed the mechanical stability of interaction with the modified Rev peptide (Fig. 1(a)). RNA oligonucleotides, equipped with 5′-hexanethiols or Rev peptide, modified with *C*-terminal cystine, were immobilized on a glass surface or AFM cantilever *via* 50 nm hetero-bis-functional NHS-PEG-Maleimide spacers (Fig. 1(b)). The peptide-functionalized AFM tip was repetitively brought into contact with the RNA-functionalized surface up to a desired cantilever deflection (trigger set point) and subsequently retracted. Successful bond association was identified from typical signatures in retraction force extension curves (FEC) that show gradual force increase from stretching PEG spacers, followed by a sudden drop in force attributed to bond rupture of the RNA–peptide complex (Fig. 2 (c)). Loading rates experienced by the bond were calculated from the slope of the curve preceding rupture. In the case of a single barrier potential, the most probable rupture force scales linearly with the log of the loading rate, from which the natural off rate k_{off} of the bond at zero force and distance between the bound and transition state along the forced reaction coordinate Δx can be determined.[23,24]

The interaction of Rev peptide with wild type RRE hairpin was probed with different retraction velocities ranging from 581 nm s^{-1} to 3.1 μm s^{-1} and with trigger set points ranging from 0.18–1.5 nN with or without a surface delay of 120 ms. In all

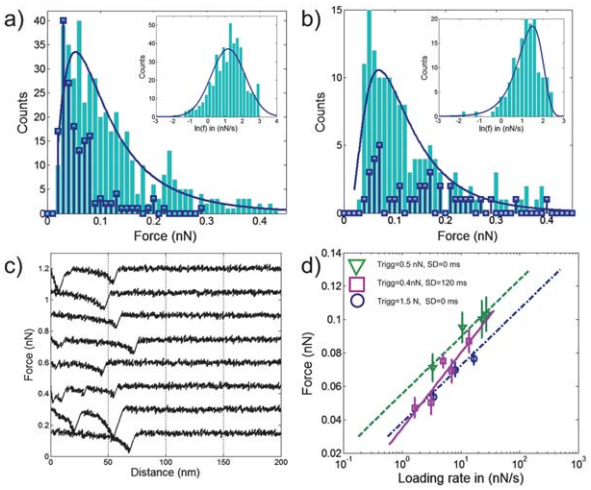

Fig. 2 Comparison of histograms for wild type RRE–Rev peptide data in the absence (light blue) and presence of 100 mM neomycin (dark blue) at a retraction velocity of 581 nm s^{-1}. Insets show the distributions of the logarithm of loading rate ln (dF/dt) with the extreme value fit. (a) Force trigger set point 1.5 nN. (b) Force trigger set point 0.5 nN. (c) Force distance curves obtained in 20 mM Tris, 100 mM KCl, pH 6.8, at a retraction velocity of 1.16 μm s^{-1}. (d) Dynamic force plots for several measurements with different force trigger set points and surface delay times.

cases measured, the histogram of rupture forces showed a wide distribution with several peaks. In these experiments many different types of interactions can contribute to the force distributions, such as: binding of Rev–peptide to high-affinity binding site, nonspecific binding, multiple bond formation and possible entanglement of PEG spacers. From control experiments where one or both binding partners were excluded in the experimental setup, it was estimated that nonspecific interactions caused by PEG spacers for a force trigger set point of 1.5 nN constitute about 10–15% of all binding events detected. For smaller trigger set points (0.2, 0.3, 0.5 nN) this percentage dropped below 5%. These nonspecific interactions together with the multiple bond formation are responsible for ruptures in the higher force regime and give rise to the long tail of the force distribution. However, for systems with reasonable affinity specific interactions are more frequent and dominate the distribution.

To estimate the kinetic parameters for the RRE_{wt}–Rev interaction we have used Bell's model.[23] The most probable values of the rupture force and the loading rate were estimated by fitting the distributions with lognormal and extreme value distributions respectively.[28] These types of distributions were found to describe the observed data profiles more reliably than the widely used normal distribution. Resulting dynamic force plots in all cases considered (with different deflection trigger set points and surface delay times, Fig. 2(d)) showed a linear dependence of force on loading rate in accordance with a single barrier transition and yielded a natural off rate at zero force $k_{off} = 5 \pm 3\ s^{-1}$. Because of the non-equilibrium nature of these experiments the exact on rate cannot be directly determined. However, a reasonable estimate can be made by assuming a diffusion controlled association process with a typical on rate of $10^8\ M^{-1}\ s^{-1}$.[27] Using this value, the equilibrium dissociation constant K_D can be estimated to be ~50 nM which agrees well with previously published data on the comparable RRE–Rev peptide interactions.[27] The inverse slopes of the linear fits of the dynamic force plots (Fig. 2 (d)) yield a potential barrier width Δx of 0.26 ± 0.02 nm. This short distance is in the range of hydrogen bonding (~1.8 Å) and much smaller than the length spanning the RNA–peptide interaction (~2.5 nm, ref. 13) and suggests the coordinated loss of the hydrogen-bonding network at the RNA–peptide interface in an all-or-none unbinding mechanism rather than gradual unzipping of the peptide from the RNA.

3.2 Influence of blocking agent neomycin

Competition experiments were performed in the presence of excess free RNA binding agent, neomycin B. Neomycin B belongs to the family of aminoglycosides antibiotics, which interact with a variety of RNA molecules, including RRE. Previous studies have shown that neomycin competes with Rev peptide for binding to the SLIIB of RRE and impairs Rev function *in vivo*,[14,15] showing its potential as a scaffold for development of novel agents against viral infection. On this particular RRE model sequence, three classes of binding sites have been detected: a site that competes with binding Rev peptide in the low micromolar range ($K_D = 1.8\ \mu M$), an adjacent non-inhibitory site, which binds neomycin with higher affinity ($K_D = 0.24\ \mu M$), allowing formation of a ternary complex with SLIIB and Rev peptide and a weaker site (or sites) ($K_D \geq 40\ \mu M$), which has been attributed to nonspecific binding.[14,15,27]

Addition of neomycin serves two purposes: first, since neomycin interferes with Rev binding, it can be used to address the specificity of RNA–peptide interaction and second, the efficiency of neomycin as a blocking agent can be assayed on the single-molecule level. The latter gives the possibility to explicitly test the AFM as a tool for single-molecule drug screening of RNA targets. Force histograms for one retraction velocity in the absence and presence of 100 mM neomycin are shown in Fig. 2(a) and (b). In the presence of neomycin the number of rupture events, assigned to unbinding of Rev–RRE_{wt} complex, were significantly reduced, which validates the interpretation of the data. However, even with a 5×10^4 over K_D excess of neomycin, which in bulk equilibrium experiments would irreversibly dissociate Rev peptide from RNA, not all binding events could be prevented. This indicates dynamic escape of the complex due to the non-equilibrium character of the measurement: fast retraction of the peptide prevents rebinding to RNA.

3.3 Influence of base mutations

To investigate the potential of AFM-SMFS in discriminating the influence of base mutations on peptide binding we probed the interaction of Rev with a mutated RRE sequence (Fig. 1(a)), in which two base pairs adjacent to the internal loop were reversed. These mutations preserve the structure of the high affinity site, but transpose functional groups necessary for Rev binding.[12]

Gel-shift binding assays indicated this mutated sequence is significantly impaired in Rev binding, displaying 10 fold lower affinity than wild type.[12] However, the mutations had no effect on the number of binding events (Fig. 3), suggesting unaltered association rates. Moreover, in contrast to the rupture force histogram of the wild type RRE which displays multiple peaks, the force histogram for the mutant RRE showed only a single sharp peak, indicating that the probability of multiple bond formation is lower due to the short life time of the RNA–peptide complex.

Analysis of the force and loading rate distributions yielded a substantially higher dissociation rate constant $k_{off} = 17 \pm 2\ s^{-1}$ implying that the dissociation rate is governing the molecular affinity. Assuming equivalent on rates for the native and mutant sequences yields an estimated $K_D = 170$ nM for the mutant interaction, *i.e.*, 4–10 fold lower affinity, consistent with the

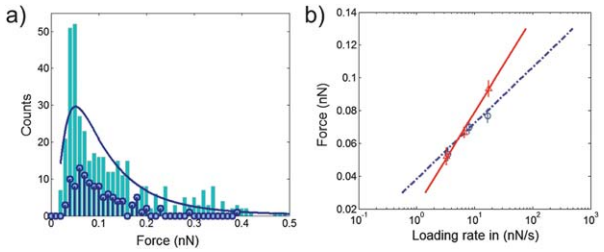

Fig. 3 (a) Histogram of rupture forces obtained for mutant RRE–Rev interaction in the absence (light blue) and presence (dark blue) of neomycin, trigger set point = 1.5 nN, $v = 581\ nm\ s^{-1}$. (b) Dynamic force plots for wild type RRE (blue circles) and mutant RRE–Rev (red triangles) interaction using the same experimental setup.

gel-shift binding assays.[12] Formation of RNA–protein complexes typically involves a multistep process characterized by initial binding, followed by conformational rearrangements of RNA and/or protein constituents that drive the complex in its final thermodynamically stable state. Apparently, shifting functional groups necessary for Rev binding does not affect the adaptive binding pathway, but loss of critical hydrogen bonds at the RNA–peptide interface[13] enhances the dissociation pathway, resulting in a larger off rate. Accordingly, the distance between the bound and transition state, derived from the linear fit of Fig. 3(b), is smaller than that for the wild type, $\Delta x = 0.166 \pm 0.005$ nm.

3.4 Influence of surface chemistry

To investigate the influence of surface immobilization and reduce nonspecific interaction we next immobilized RRE directly to a gold surface using 5′-hexanethiol. This experimental setup has two benefits. First, it should decrease rupture events arising from PEG entanglement between the tip and the surface, and second, the enduring liquid flow needed to flush out neomycin should not drastically affect the RNA–surface coupling since the covalent bond between the 5′-thiol of the RNA and gold surface is much stronger.

Measurements were performed with velocities ranging from 1160–3100 nm s^{-1}, a trigger set point of 0.2 nN and a surface delay of 120 ms. The small trigger set point was chosen to reduce nonspecific surface interactions and the long surface delay time to insure proper bond formation between RRE and Rev peptide. Force curves showed two distinct interaction regimes, nonspecific surface interactions at distances below ~20 nm, and a single bond rupture at a larger distance (Fig. 4(a)). Thus, compared to the data acquired with RRE immobilized to the surface *via* PEG linkers, the rupture force distributions shown in Fig. 4(b) were relatively narrow and exhibited only a single maximum (note the maximum observed rupture force is 0.25 pN whereas for PEG-immobilized RRE the maximum observed force value is 0.5 nN). The absence of large rupture forces indicates that there is no multiple bond formation as well as no PEG-entanglement. The blocking experiment with neomycin was performed as with PEG-immobilized RRE, *i.e.*, by injecting a 100 mM solution of neomycin dissolved in standard buffer. In this case blocking with neomycin was even more efficient, resulting in 6-fold reduction in rupture events (Fig. 4(b), middle). Moreover, neomycin could be washed away efficiently, resulting in almost complete revival of the initial rupture force distribution (Fig. 4(b), bottom).

So far usage of long PEG spacers has been proven successful for probing biomolecular interactions on a variety of DNA–DNA, DNA–peptide and ligand–receptor pairs, and has thus emerged as the preferred method.[7,16–18,29,30] However, our results indicate that for the purpose of single-molecule drug screening on RNA targets, linking of RNA molecules to the surface devoid of PEGs might be more favorable. Also, the 2D contour plot of rupture forces plotted against the effective spring constant κ (Fig. 5(a)) showed only a single peak indicating a single-binding mode between Rev and wild type RRE.[7,25] Since this experimental setup revealed only a single barrier transition and no multiple bond formation, this dataset was subjected to further data analysis.

3.5 Comparison of theoretical models

For the analysis of the RRE(Au)–Rev dataset using Bell's model, we fitted the force and loading rate distributions with the appropriate probability density function as shown in Fig. 5(b) (full line). The maxima of the fitted force and loading rate distributions for each retract velocity v were subsequently plotted in the dynamic force plot shown in Fig. 5(c). The linear fit of this

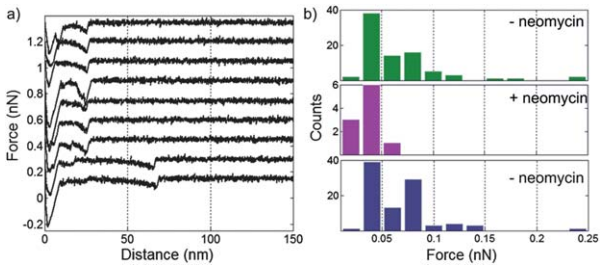

Fig. 4 (a) Force curves obtained with RRE oligonucleotides coupled directly to a gold surface *via* a 5′-thiol label. (b) Influence of neomycin. Top: force distribution obtained in standard buffer; middle: force distribution obtained in standard buffer containing 100 mM neomycin; bottom: force distribution obtained after flushing the liquid cell of the AFM with standard buffer.

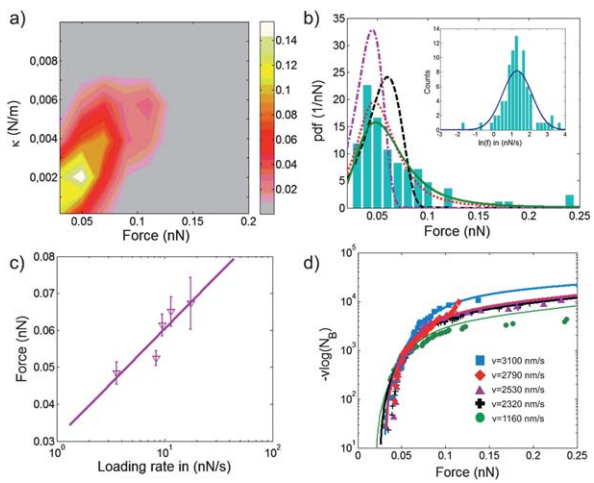

Fig. 5 (a) 2D contour plot with histogram of rupture forces plotted against the histogram of effective spring constants. The graph shows one strong peak at $\kappa \approx 0.0026$ N m^{-1}, indicating the existence of a single binding mode. (b) Comparison of the distributions calculated with different methods: (–) log–logistic fit of the rupture force distribution used to determine the most probable force; (---) Bell's model calculated from the parameters obtained from the dynamic force plot (a); (···) Probability density function of rupture forces calculated according to the model of Raible *et al.*;[23] (---) Bell's model calculated from the parameters obtained using the log–logistic fit of the rupture force distributions. The inset shows the distribution of loading rates ln (dF/dt). (c) Dynamic force plot obtained from the most probable forces and loading rates of RRE–Rev interaction with RRE immobilized on gold. (d) Functions $-v\ln(pN_E(F))$ for different pulling velocities v and fitted with model functions proposed by Raible *et al.*[23] Each data point corresponds to one recorded rupture event.

plot yielded values for the natural off rate $k_{off} = 7 \pm 3\ s^{-1}$ and barrier width $\Delta x = 0.32 \pm 0.02$ nm. These values are very close to those obtained with RRE immobilized to the surface *via* PEG spacers.

We next derived relevant parameters by using the theoretical framework of Raible *et al.*[25] In the case of a single barrier model the quantities for the probability of bond survival $-v\ln(pN_E(F))$ should collapse onto a single curve for all retraction velocities, from which k_{off} and Δx can be obtained by fitting. If this is not the case the discrepancy can be remedied by averaging the observed survival probabilities with respect to the probability distribution of k_{off} and Δx instead of using single values. The rationale for this approach is that parameter distributions rather than single values can compensate for the variations in the measured dissociation rate and the potential width arising from, for example, changes of the local chemical environment, the orientation of the molecular complex during pulling, pulling on multiple bonds or pulling on different types of bonds (specific or nonspecific).[23] Raible *et al.* showed that the model is not very sensitive to small variations in k_{off} but it is very sensitive to variations in Δx. Therefore, it is sufficient to average the experimental survival probability over the dissociation length α, which in the framework of Raible *et al.*[25] is defined in units of thermal energy as

$$\alpha = \Delta x / k_B T$$

where α is sampled from a Gaussian distribution with mean α_μ and standard deviation σ_α (see Materials and methods). If the data represent a single-barrier transition, sets of fitting parameters (k_{off}, α_μ, σ_α) should have approximately the same values for all retract velocities. The data analysis with the model developed by Raible *et al.* is presented in Fig. 5(d). All of the observed experimental curves could be fitted with approximately the same parameters: $k_{off} \approx 5.4\ s^{-1}$, $\Delta x \approx 0.25$ nm and $\sigma_\alpha \approx 0.1$ nm. This result indicates that the data are consistent with a single binding mode with heterogeneity of the chemical bond effectuated in the dispersion of the chemical bond length. The corresponding probability density function calculated using these parameter values is shown in Fig. 5(b).

4. Conclusions

Herein, we have investigated the specific interaction of the RNA recognition motif of Rev and its viral mRNA target, RRE, for the first time at the single-molecule level by AFM-SMFS. The molecular binding forces observed for single RNA–peptide interactions underscore the specificity deduced from bulk experiments, and also provided some details of the dissociation pathway and influence of base mutations that were not revealed from the bulk experiments. Competition experiments with neomycin proved the specificity of measured unbinding forces as well as neomycin's blocking efficiency, showing the potential of AFM-SMFS as a tool for single-molecule drug screening. Moreover we showed that choice of surface immobilization can be critical for the blocking efficiency by small molecules. With RRE immobilized to the surface *via* PEG spacers addition of neomycin showed a reduction in the number of rupture events of a factor of 2–3, whereas when RRE was coupled directly to the gold surface, the number of binding events was further reduced to a factor of 6. The calculated bond parameters extracted from the corresponding dynamic force plots were approximately the same for all datasets and were independent of the experimental setup or ramping conditions. Using the classic Bell–Evans approach[23,24] the natural off rate of the wild type RNA–peptide bond at zero force was estimated to be $k_{off} \approx 5\ s^{-1}$ which is in good agreement with previously reported off-rates for the same system.[27] The obtained distance from the bound to the transition state Δx was ~0.26 nm. For the dataset where RRE was immobilized to the gold surface, the theoretical model suggested by Raible *et al.*[25] could be tested. The obtained values of off-rate and the potential width utilizing this model were $k_{off} \approx 5.4\ s^{-1}$ and $\Delta x \approx 0.25$ nm. These values compare very well to the values obtained by the less elaborate and complicated Bell–Evans approach, which is encouraging for using this approach in rapid single-molecule drug screening of RNA targets by AFM-SMFS.

However, compared to other types of interaction pairs, *i.e.*, DNA–DNA, DNA–peptide and protein–peptide, the distribution of rupture forces of the RNA–peptide interaction pair seems to be larger, which might originate from a higher propensity of alternative and nonspecific binding events, born out of the higher flexibility and plasticity of RNA. The potential to distinguish different binding modes of single RNA–protein interaction by AFM-SMFS using more elaborate theoretical frameworks as developed by Raible *et al.* could therefore prove to be extremely useful in resolving multivalent interactions, which is an intricate property of the adaptive binding mechanism of RNA–ligand recognition.

Acknowledgements

The authors wish to acknowledge financial support from the 6th framework Program within the project Functional and Structural Genomics of Viral RNA: FSG-V-RNA. Dr Peter Schön is acknowledged for helpful discussions. We are also grateful to Prof. Dr Jan Van Hest and Dr Dennis Löwik for providing the Rev peptide.

Notes and references

1 Y. F. Dufrêne and P. Hinterdorfer, *Pfluegers Arch.*, 2008, **456**, 237–245.
2 D. J. Müller and Y. F. Dufrêne, *Nat. Nanotechnol.*, 2008, **3**, 261–269.
3 E. M. Puchner and H. E. Gaub, *Curr. Opin. Struct. Biol.*, 2009, **19**, 605–614.
4 S. Marsden, M. Nardellin, P. Linder and J. E. G. McCarthy, *J. Mol. Biol.*, 2006, **361**, 327–335.
5 A. Fuhrmann, J. C. Schoening, D. Anselmetti, D. Staiger and R. Ros, *Biophys. J.*, 2009, **96**, 5030–5039.
6 V. W. Pollard and M. H. Malim, *Annu. Rev. Microbiol.*, 1998, **52**, 491–532.
7 A. D. Frankel and J. A. T. Young, *Annu. Rev. Biochem.*, 1998, **67**, 1–25.
8 M. L. Zapp and M. R. Green, *Nature*, 1989, **342**, 714–716.
9 M. H. Malim and B. R. Cullen, *Cell*, 1991, **58**, 205–214.
10 D. A. Mann, I. Mikkaelian, R. W. Zemmel, S. M. Green, A. D. Lowe, T. Kimura, M. Singh, P. J. G. Butler, M. J. Gait and J. Karn, *J. Mol. Biol.*, 1994, **241**, 193–197.
11 R. W. Zemmel, A. C. Kelley, J. Karn and P. J. G. Butler, *J. Mol. Biol.*, 1996, **258**, 763–777.
12 P. C. Brice, A. C. Kelley and P. J. G. Butler, *Nucleic Acids Res.*, 1999, **27**, 2080–2085.

13 J. L. Battiste, H. Mao, N. S. Rao, R. Tan, D. R. Muhandiram, L. E. Kay, A. D. Frankel and J. R. Williamson, *Science*, 1996, **273**, 1547–1551.
14 M. L. Zapp, S. Stern and M. R. Green, *Cell*, 1993, **74**, 969–978.
15 S. R. Kirk, N. W. Luedtke and Y. Tor, *J. Am. Chem. Soc.*, 2000, **122**, 980–981.
16 T. Strunz, K. Oroszlan, R. Schäfer and H. J. Güntherodt, *Proc. Natl. Acad. Sci. U. S. A.*, 1999, **96**, 11277–11282.
17 J. L. Zimmermann, T. Nicolaus, G. Neuert and K. Blank, *Nat. Protoc.*, 2010, **5**, 975–985.
18 H. A. Heus, E. M. Puchner, A. F. M. Vugt-Jonker, J. L. Zimmermann and H. E. Gaub, *Anal. Biochem.*, 2011, **414**, 1–6.
19 M. Hegner, P. Wagner and G. Semenza, *Surf. Sci.*, 1993, **291**, 39–46.
20 J. te Riet, T. Smit, J. W. Gerritsen, A. Cambi, J. A. A. W. Elemans, C. G. Figdor and S. Speller, *Langmuir*, 2010, **26**, 6357–6366.
21 H. J. Butt and M. Jaschke, *Nanotechnology*, 1995, **6**, 1–7.
22 E. L. Florin, M. Rief, H. Lehman, M. Ludwig, C. Dornmair, V. T. Moy and H. E. Gaub, *Biosens. Bioelectron.*, 1995, **10**, 895–901.
23 G. I. Bell, *Science*, 1978, **200**, 618–627.
24 E. Evans, *Annu. Rev. Biophys. Biomol. Struct.*, 2001, **30**, 105–128.
25 M. Raible, M. Evstigneev, F. W. Bartels, R. Eckel, M. Nguyen-Duong, R. Merkel, R. Ros, D. Anslemetti and P. Reimann, *Biophys. J.*, 2006, **90**, 3851–3864.
26 K. S. Cook, G. J. Fisk, J. Hauber, N. Usman, T. J. Daly and J. R. Rusche, *Nucleic Acids Res.*, 1991, **19**, 1577–1583.
27 K. A. Lacourciere, J. T. Stivers and J. P. Marino, *Biochemistry*, 2000, **39**, 5630–5641.
28 R. M. Feldman and C. Valdez-Flores, *Applied Probability and Stochastic Processes*, Springer, 2nd edn, 2010.
29 U. Dammer, M. Hegner, D. Anselmetti, P. Wagner, M. Dreier, W. Huber and H.-J. Guntherodt, *Biophys. J.*, 1996, **70**, 2437–2441.
30 R. Eckel, S. D. Wilking, A. Becker, N. Sewald, R. Ros and D. Anselmetti, *Angew. Chem., Int. Ed.*, 2005, **44**, 3921–3924.